Ejecta Pulsing of Subscale Solid Propellant Rocket Motors

Richard L. Lovine*
Aerojet Tactical Systems, Sacramento, California
and
Joseph D. Baum† and Jay N. Levine ‡
Air Force Rocket Propulsion Laboratory/DYC, Edwards AFB, California

This paper presents results of an experimental and analytical study of ejecta pulsing. A series of motor firings was conducted in which spheres of different sizes and materials were ejected through the nozzle to simulate in-flight partial nozzle blockage due to igniter, propellant, or other combustion chamber material fragments. Simple laboratory-scale solid rocket motors with full- and partial-length grains were utilized. All of the motors tested were triggered into sustained nonlinear instability. A simple analysis was developed to calculate the velocity of the ejecta and pulse duration. Good agreement between predicted and measured pulse durations was obtained. Two methods were developed for predicting initial ejecta induced pulse amplitudes: 1) a simple model based on linear wave propagation theory and the assumption of quasisteady nozzle behavior, and 2) a numerical model which utilizes the quasisteady nozzle assumption to provide a nozzle entrance boundary condition to a comprehensive combustion chamber nonlinear instability analysis. Comparisons of theoretical predictions with experimental data for both pulse amplitude and the motor response to pulsing are presented. The nonlinear instability analysis was found to be capable of predicting most of the nonlinear behavior observed in motor response to ejecta pulsing. Good agreement between measured and predicted initial pulse (amplitude and harmonic content), waveform evolution, growth and decay rates, and dc shift was obtained.

Introduction

SOLID propellant rocket motors that have a high length-to-diameter ratio are known to be susceptible to nonlinear axial mode instabilities. Such instabilities are characterized by large-amplitude oscillations having steep-fronted, shock-type waveforms, and are often accompanied by significant mean pressure increases. By definition, nonlinear instability is the triggering of an instability by a finite amplitude disturbance in a system that is otherwise linearly stable, i.e., stable to infinitesimal disturbances. In solid rocket motors, the primary source of random finite amplitude pressure disturbances (other than low-amplitude turbulence and combustion noise) is the transient reduction in throat area that results from the ejection of igniter, propellant, or other combustion chamber material fragments through the nozzle.

A variety of pulser units have been designed to facilitate laboratory investigations of nonlinear instability.[1-3] All of these designs share the common feature of inducing disturbances by discharging gaseous combustion products (at a controlled rate) into the combustion chamber. The point of discharge is usually the fore end of the motor as opposed to the aft-end point of origination for naturally induced nozzle ejecta pulses. Although laboratory pulse units have been widely used,[4] the physical mechanisms responsible for pulse initiation of nonlinear instability are not yet fully understood.

The ejecta pulsing investigation described herein is part of a large effort to develop guidelines for conducting valid solid rocket motor pulse tests and models for predicting both pulse characteristics and motor reponse to pulsing. The development of models capable of the accurate, a priori prediction of mass and energy flow rates produced by pyrotechnic, piston, and low brisance pulsers, as well as the waveforms produced by these pulsers inside a solid propellant rocket motor, has been reported previously.[5] Ballistic models for these pulsers were developed utilizing a simple lumped volume treatment. The mass and energy flow rates calculated using these pulser performance models were utilized as boundary conditions for the chamber flow problem, which was solved using a modified nonlinear combustion instability model. Results demonstrating the ability of the developed pulser/chamber model to accurately predict both initial pulse amplitude and waveform, under cold flow conditions[6] and under actual solid rocket motor firing conditions,[7] have been presented. The ability to accurately predict the resulting wave development in the chamber (amplitude, waveform, dc shift, and growth or decay rates) also has been demonstrated.[7]

The present effort involves both experiments and the development of models designed to simulate ejection of combustion chamber material through the nozzle. Pulse tests were conducted in which spheres of different densities and sizes were ejected at the head end. The test data were used to identify the characteristics of oscillations resulting from nozzle ejecta and their capability to initiate sustained pressure oscillation in a solid rocket combustion chamber. The test data were also used to examine the validity of the concurrently developed models.

The modeling work consisted of several parts. First, a simplified model was developed to calculate the motion of an ejecta through the nozzle. Two methods for predicting the resulting pulse amplitude were then developed. Based on a linearized analysis, a semiempirical method that predicts the amplitude of ejecta induced pulses at the nozzle entrance was developed. The second approach utilized an existing comprehensive model of nonlinear combustion instability[8] modified to accept a time-dependent Mach number boundary condition at the nozzle entrance, as determined from the calculated throat constriction time history. Comparisons of predictions obtained utilizing the first model and the measured initial pulse amplitudes were presented. Finally, it was shown that the modified nonlinear instability analysis is capable of accurately predicting the initial pulse amplitude

Presented as Paper 83-0578 at the AIAA 21st Aerospace Sciences Meeting, Reno, Nev., Jan. 10-13, 1983; submitted Jan. 28, 1983; revision received Dec. 19, 1983.

*Engineering Specialist. Member AIAA.
†Research Physical Scientist. Member AIAA.
‡Research Physical Scientist.

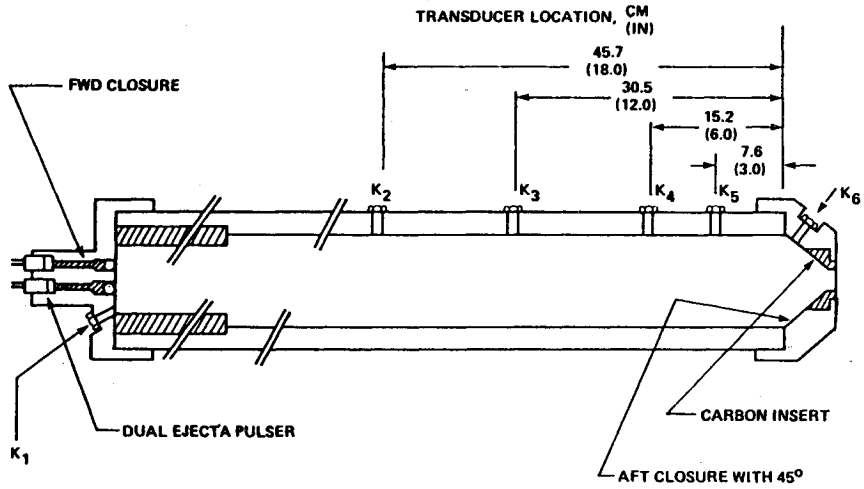

Fig. 1 Schematic of the ejecta pulse test apparatus.

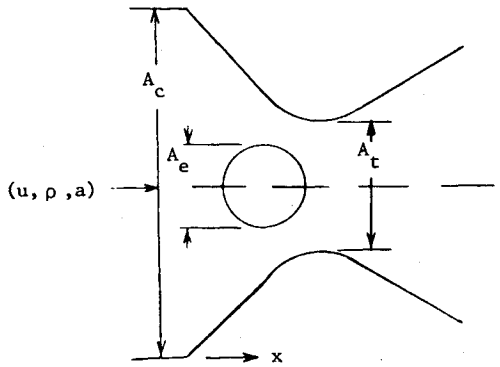

Fig. 2 Reference areas for ejecta pulsing.

and the motor response to pulsing, as observed in waveform evolution, growth rate, and mean chamber pressure.

Experimental Apparatus

The ejecta pulse test apparatus consisted of a thick-walled combustion chamber in which either partial- or full-length cylindrical grains were loaded and fired. Two ejecta pulsers were attached to the fore end of the chamber. A schematic of the ejecta pulse test apparatus is shown in Fig. 1. The combustion chamber had an overall length of 1.22 m (48 in.) and an internal case diameter of 5.71 cm (2.25 in.). Nozzle entrance and exit angles were 45 and 15 deg, respectively. The partial-length cylindrical grains were partially recessed into the case. Thus, at some time toward the end of the firing, a flush grain configuration was achieved. Prior to this time, the grain represented an area constriction. After this time, the grain was recessed relative to the case wall. At predetermined times during the firing, the pulsers ejected a sphere into the chamber which was carried out through the nozzle by the flow of combustion gases. To simulate the range of material densities found in combustion chambers, a series of tests was carried out using spheres made from RTV[IM] rubber (utilized in most of the tests), nylon, teflon, and steel.

The pressure oscillations in the motor were recorded at six axial locations using Kistler 7031 piezoelectric pressure transducers. The chamber sidewall was instrumented with four close-coupled pressure transducers; one transducer was located at the fore-end closure and one in the convergent section of the nozzle. The transducer ports were machined so that the transducer diaphragms were offset by 0.125 in. This cavity was potted with vulcanized rubber (RTV) which is utilized to provide thermal shielding of the pressure transducers. In its mounted configuration, the transducer had a resonant frequency of about 65 kHz, as determined by shock tube tests. With this high value for resonant frequencies, the amplification error should be less than 2% for a 12 kHz signal.

Ejecta Trajectory

The prediction of the pressure pulse waveform that results from the transient partial blockage of the nozzle (termed nozzle ejecta) requires calculation of the nozzle constriction as a function of time. Therefore, it is the ejecta velocity as well as its physical size that determines the pressure pulse waveform. The equation of motion for the ejecta is $F=m\,(\mathrm{d}u_e/\mathrm{d}t)$, where m is the ejecta mass, u_e the ejecta velocity, and F the force acting on the particle. For a particle whose density is large compared to that of the gas medium, and when the fluid acceleration is low, the equation of motion is written as

$$m\frac{\mathrm{d}u_e}{\mathrm{d}t} = \tfrac{1}{2}c_d\rho(u-u_e)\,|u-u_e|A_e \qquad (1)$$

where u is the gas velocity, c_d the drag coefficient, ρ the gas density, and A_e the ejecta cross-sectional area.

The force acting on the ejecta is a combination of viscous drag and pressure differences across the ejecta surface (termed pressure drag). At high velocities the pressure drag is largely a result of flow separation which causes a nonuniform pressure distribution over the surface of the body. Measured drag coefficients are usually presented as a plot of total drag (viscous plus pressure) as a function of Reynolds number. Schlichting[9] presented sphere drag for both compressible and incompressible flow. For incompressible flow, the drag coefficient is approximately equal to 0.4 in the range of Reynolds numbers from 10^3 to 3×10^5. At the critical Reynolds number of 3×10^5 the drag coefficient drops sharply. Compressibility effects act to increase both the drag coefficient and the critical Reynolds number. For Mach numbers in the range of 0.8 to 4.5 and Reynolds numbers in the range of 2 to 9×10^5, the drag coefficient is insensitive to Reynolds number and its value is approximately 0.65-0.75. Experimental data obtained during ejecta pulse tests imply average velocities in the throat region of about 600-3000 in./s, depending on the ejecta density, initial injection velocity, and motor mean pressure. With these values, the Reynolds number would be in the range of 2×10^4 to 10^6. This range encompasses the critical Reynolds number for incompressible flow.

The existence of strong, mean flow pressure gradients in the nozzle may have a significant influence on the drag force. Nevertheless, for the sake of simplicity, such potential pressure gradient effects have not been considered in the present work and only the conventional drag force was incorporated in the ejecta trajectory analysis. Pressure measurements at the nozzle entrance then were used to

estimate the appropriate value of the drag coefficient. Details of the approximate analysis are described later in the paper.

Ejecta Pulse Modeling

The nozzle geometry during spherical ejecta passage is shown in Fig. 2, where A_c is the nozzle entrance area, A_e the ejecta area, A_t, the throat area, a sonic velocity, u gas velocity and, ρ the gas density.

A simple model for calculating the amplitude of the ejecta induced pulse at the nozzle entrance plane was developed. The assumptions involved were: the flow in the nozzle is one-dimensional and isentropic and the ejecta only affects the instantaneous nozzle throat area. As the ejecta enters the throat, a series of weak compression waves propagates upstream toward the nozzle entrance slowing the flow. After the maximum diameter of the ejecta passes through the throat, a series of expansion waves now propagates toward the nozzle entrance, at a slightly higher velocity than the compression waves. Using linear wave propagation theory, the ratio of the instantaneous pressure at the nozzle entrance, p, to the initial undisturbed entrance pressure, p_1, eventually can be expressed as

$$\frac{p}{p_1} = \left[\left(1+\frac{\gamma-1}{2}M_1^2\right)\Big/\left(1+\frac{\gamma-1}{2}M^2\right)\right]^{(2\gamma)/(\gamma-1)} \tag{2}$$

Thus, the instantaneous pressure is determined once the nozzle entrance Mach number M is known. In order to determine M, a quasisteady nozzle behavior was assumed, i.e., the instantaneous Mach number can be calculated using steady-state relations. The initial undisturbed nozzle entrance Mach number is given by

$$M_1 = J\left[\left(1+\frac{\gamma-1}{2}M_1^2\right)\left(\frac{2}{\gamma+1}\right)\right]^{(\gamma+1)/2(\gamma-1)} \tag{3}$$

where $J=A_t/A_c$ is the initial undisturbed value of the nozzle constriction ratio. The Mach number at the nozzle entrance plane during the ejecta passage is then given by Eq. (3) with M_1 replaced by M and J by $J(1-f_b)$ (where f_b is the fraction of the throat area blocked at any instant). The quasisteady nozzle assumption should be most applicable to larger, slower-moving ejecta. As the ejecta velocity increases, the quasisteady assumption leads to overprediction of the pulse amplitude.

Equation (3) is a transcendental equation for M_1 as a function of J. However, if it is assumed that $0.5\,(\gamma-1)M_1^2$ is small compared with one (M_1 is typically on the order of 0.1 and $\gamma=1.23$) M_1 and M can be expressed as

$$M_1 = J\left(\frac{2}{\gamma+1}\right)^{(\gamma+1)/2(\gamma-1)}$$
$$M = J(1-f_b)\left(\frac{2}{\gamma+1}\right)^{(\gamma+1)/2(\gamma-1)} \tag{4}$$

Inserting Eqs. (4) into Eq. (2), and neglecting terms on the order of $0.1J$, yields the following expression for pulse amplitude

$$\frac{p_1-p}{p_1} = \frac{\delta p}{p_1} = \left[\gamma\left(\frac{2}{\gamma+1}\right)^{(\gamma+1)/2(\gamma-1)}\right] f_b J \tag{5}$$

With an isentropic exponent, γ equal to 1.2, Eq. (5) becomes

$$\delta p/p_1 = 0.71 f_b J \tag{6}$$

Thus, this simple model predicts that the pulse amplitude is proportional to the product of the initial constriction ratio and the fraction of the throat area blocked by the ejecta, and provides a good basis for data correlation. Comparison of predictions obtained utilizing this model with experimental data is shown later in the paper.

A second approach for calculating ejecta pulse amplitudes was developed by modifying an existing nonlinear combustion instability analysis.[8] This computer program, which solves the coupled nonlinear partial differential equations that govern the one-dimensional, two phase flow in variable cross-sectional area solid rocket motors and the transient combustion of the solid propellant, was modified to accept a time-dependent Mach number boundary condition at the nozzle entrance.

In this approach, the ejecta trajectory is calculated as described previously. The quasisteady assumption was retained, thus the nozzle entrance Mach number is given by Eq. (3) with J replaced by the instantaneous nozzle constriction ratio. The program calculates the flow variables at interior mesh points using an advanced shock-capturing finite difference integration technique, while the method of characteristics is employed at the boundaries. Thus, at the nozzle entrance, the specified Mach number boundary condition that describes the effect of ejecta passage through the nozzle (i.e., the generation of compression and expansion waves) is conveyed to the combustion chamber via a left-running (upstream) characteristic.

Since the nonlinear combustion instability analysis treats the whole problem (i.e., the time evolution of oscillations in the motor, coupled with the propellant response), this approach is not limited to the calculation of the ejecta induced initial pulse amplitude. It is also capable of calculating the waveforms of the pulse and the resulting motor behavior, i.e., growth or decay of the disturbance. The ability to model the nonlinear response of solid rocket motors to pulsing has been demonstrated previously for low brisance, piston, and pyrotechnic pulsers located at the head end of the chamber.[7] A comparison between predictions and experimental data obtained by ejecta pulsing subscale rocket motors is presented in the following sections.

Experimental Results and Comparison with Theory

Experiments

A series of motor firings was carried out using the previously described test apparatus and instrumentation. The results of nine of these tests are considered herein. AP-HTPB propellant grains with lengths varying from 8 to 48 in., initial i.d. of 1.25 in. and o.d. of 2.375 in. were tested. Spherical ejecta of different materials were employed to study the effect

Table 1 Ejecta pulser test conditions

Test No.	Grain length, in.	Ejecta size, in.	Fraction blocked	Ejecta material	Chamber pressure, psi
1	19.7	0.4375	0.364	RTV	990
2	16	0.4375	0.45	RTV	832
3	12	0.375	0.482	RTV	993
4	8	0.375	0.726	RTV	900
5	16	0.4375, 0.60	0.369, 0.694	Nylon	905, 877
6	16	0.4375, 0.60	0.369, 0.694	Teflon	805, 856
7	16	0.4375, 0.60	0.369, 0.694	Steel	751,811
8	32	0.5	0.284	Teflon	1085
9	48	0.872	0.575	Teflon	1200

Table 2 Ejecta density variation tests

Test No.	Pulse	Ejecta material	Density, lb/in.^{3}	Diameter, in.	f_b(max)	Mean pressure, psi	Pulse amplitude, psi	Pulse duration, ms
5	1	Nylon	0.039	0.4375	0.369	905	15.0	0.34
	2	Nylon	0.039	0.60	0.694	877	39.7	0.59
6	1	Teflon	0.075	0.4375	0.369	805	14.9	0.49
	2	Teflon	0.075	0.60	0.694	856	38.4	0.74
7	1	Steel	0.275	0.4375	0.369	751	17.8	0.88
	2	Steel	0.275	0.60	0.694	811	34.4	1.33

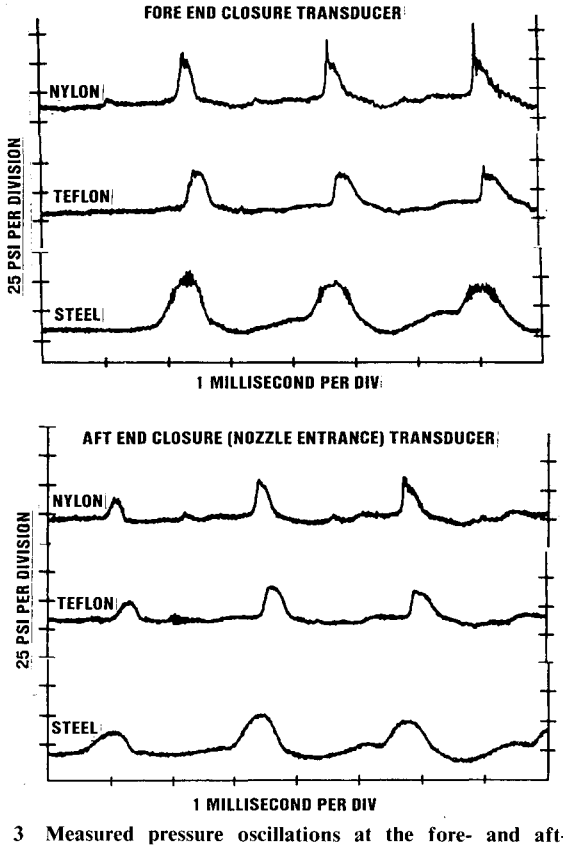

Fig. 3 Measured pressure oscillations at the fore- and aft-end closures induced by the first pulse, tests 5-7.

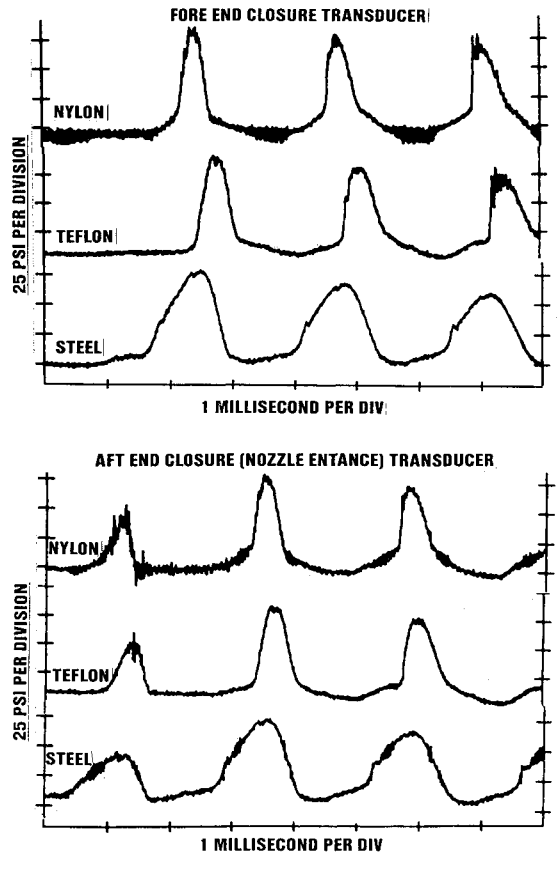

Fig. 4 Measured pressure oscillations at the fore- and aft-end closures induced by the second pulse, tests 5-7.

of density variations. The materials consisted of nylon, rubber, teflon, and steel, having densities of 0.039, 0.040, 0.075, and 0.275 lb/in.^{3}, respectively. Ejecta size was also varied, resulting in throat blockage ranging from 32 to 69%. The test conditions are summarized in Table 1.

Pulse Duration—Ejecta Trajectory Model Evaluation

Tests 5, 6, and 7, in which materials of three widely different densities were employed (nylon, teflon, and steel, respectively), provided an excellent means for evaluating the capability of the previously described approximate model to calculate the ejecta trajectory (velocity) as it transits the throat. These tests also provided a basis for assessing the effect of ejecta density variation upon the resulting pulse amplitude and waveform. The initial pulsed waveforms measured at the nozzle entrance and at the chamber fore-end closure are shown in Figs. 3 and 4. The test results are summarized in Table 2. The pulse amplitude and duration listed in Table 2 refer to the initial disturbance at the nozzle entrance. Later measurements of the pulse, after it has been reflected from either the fore end or the nozzle end, show that at that time the pulse has approximately doubled its initial amplitude. This is a consequence of the reflection process for a traveling wave.

Using the previously described methodology, ejecta trajectory calculations were performed for two assumed values of ejecta initial velocity, and three different values of the drag coefficient. The calculated pulse durations (time for ejecta to pass the throat plane) are tabulated in Table 3. From a comparison of Tables 2 and 3, it is concluded that: pulse duration is only weakly dependent upon drag coefficient and initial ejecta entrance velocity; and that a reasonable choice of these parameters results in calculated pulse durations that are approximately correct. The resulting pulse amplitude is also relatively insensitive to ejecta velocity (except, as will be pointed out later, for very fast ejecta velocities). Thus, efforts to improve upon the present simple ejecta trajectory prediction methodology do not appear to be warranted.

For present purposes, the remainder of the ejecta trajectory calculations were carried out using an entrance velocity of 100 in./s and a drag coefficient equal to 0.6. Using these values, the fraction of throat area blocked was calculated. Figures 5

and 6 show the variation of fraction of throat area blocked as a function of time for tests 5-7. The ejecta velocity increases monotonically with time as it passes through the nozzle (barring collision with the nozzle walls). Thus, the time interval from initial blockage to maximum throat blockage is longer than the time required to return from maximum blockage to the original cleared throat area. Hence, the initial waveform of the ejecta pulse, measured at the nozzle entrance, should have a shallower front (rise) and a steeper back (decay). The initial measured waveforms all have this characteristic (which is especially evident with the slower steel balls); however, nonlinear wave propagation effects (i.e., steepening, viscosity, viscous wall losses, etc., rapidly cause the wave shape to change to a steeper wave front and a shallower back.

Evaluation of Pulse Amplitude Prediction Models

Semiempirical Model

The experimental ejecta pulse test results that are shown in Table 1 were also used to examine the validity of the previously described pulse amplitude prediction models. Since Eq. (6) predicts that the pulse amplitude is proportional to the product f_bJ, the measured pulse amplitudes were plotted as a function of f_bJ (Fig. 7). The data fall below the theoretically predicted line ($\delta p/p = 0.71\, f_bJ$), and are reasonably correlated by $\delta p/p = 0.6 f_bJ$. The overprediction of pulse amplitude is most likely a result of imposing a quasisteady approximation in the model development. As expected, the greatest deviations from the predicted values are for the smallest, fastest moving ejecta. The two lowest pulse amplitudes shown in Fig. 7 (having the largest deviations) were obtained using smaller rubber ejecta injected into the motor at higher velocities than the other ejecta (larger quantities of black powder were utilized in the ejecta pulser unit). The measured pulse durations of these ejecta at the nozzle entrance were only 0.3 ms. Conversely, the two nylon ejecta data points at f_bJ values of 0.035 and 0.0435 were obtained for larger (slower) ejecta in a 3.0-in-diam test motor. Until a more accurate, fully transient, two-dimensional model describing ejecta motion through a nozzle is developed, the relation $\delta p/p = 0.4 f_bJ$ should probably be used instead of the aforementioned relation when ejecta pulse durations are expected to be in the range of 0.2 to 0.4 ms.

In full-scale motors, the larger ejecta necessary to produce reasonable pulse amplitudes should have dwell times on the order of a millisecond, and the relation $\delta p/p = 0.6 f_bJ$ should yield reasonably accurate predictions of initial pulse amplitude.

Numerical Model

The task of defining pulse amplitude is not as straightforward as it seems, since the amplitude of the pulse varies with axial location in the motor. Thus, simple correlations of predicted and measured "pulse amplitude" values cannot tell the whole story. It has already been mentioned that when a traveling pulse reflects from the head-end closure, its amplitude at the head-end is approximately double its amplitude at the middle of the chamber. Several other physical processes involved in wave propagation can affect the measured pulse amplitude. One such effect is the formation of a system of multiple shock waves that results from the partial reflection of the pulse from area or grain discontinuities or the continuous partial reflection/transmission of a pulse traveling in a variable cross-section area chamber.

Since the numerical model includes the operative nonlinear wave propagation mechanisms, it can treat the pulse amplitude prediction problem without the necessity of defining a single value for "pulse amplitude." In addition, being a complete nonlinear combustion analysis, the numerical approach also can be used to predict the motor response to ejecta pulsing (see next subsection).

Although the present numerical model has the above advantages, it still employs a quasisteady assumption in specifying the time-dependent Mach number boundary condition at the nozzle entrance. Thus, the nozzle ballistic analysis was empirically corrected in order to obtain good agreement between the measured and predicted pulse amplitudes at the nozzle entrance. The corrected pulse amplitudes were utilized as a nozzle entrance boundary condition. The objective of this analysis was to evaluate the ability of the nonlinear combustion instability analysis to properly predict the spatial and temporal wave propagation in the chamber, given accurate boundary conditions at the aft end. This capability was evaluated based upon comparison of the experimental and theoretical results at the fore end. The comparison between predictions and measurements for the first wave cycle is shown on Table 4. Comparisons of the time evolution of the pressure waveforms are shown in Figs. 8-11. The predicted and measured pulse amplitudes at the fore end were in excellent agreement, as shown in Table 4. The results also verified the ability of the analysis to predict the observed

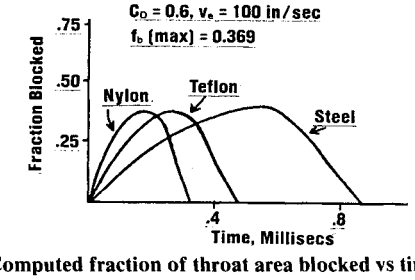

Fig. 5 Computed fraction of throat area blocked vs time, first pulse, tests 5-7.

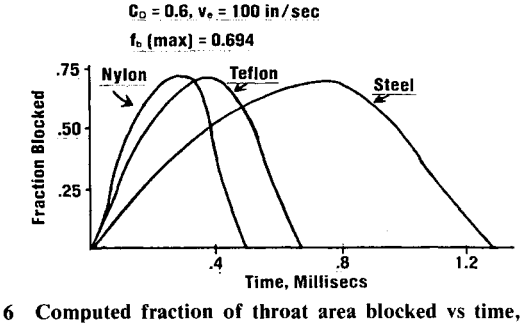

Fig. 6 Computed fraction of throat area blocked vs time, second pulse, tests 5-7.

Table 3 Computed pulse durations

Test No.	Ejecta density, lb/in.	Ejecta diameter, in.	$v_e = 100$ in./s C_D	Duration, ms	$v_e = 300$ in./s C_D	Duration, ms
5	0.039	0.4375	0.5	0.36	0.4	0.40
			0.6	0.34	0.5	0.36
			0.7	0.32	0.6	0.32
		0.60	0.5	0.54	0.4	0.58
			0.6	0.50	0.5	0.52
			0.7	0.46	0.6	0.50
6	0.075	0.4375	0.5	0.52	0.4	0.56
			0.6	0.48	0.5	0.50
			0.7	0.44	0.6	0.46
		0.60	0.5	0.74	0.4	0.78
			0.6	0.66	0.5	0.70
			0.7	0.64	0.6	0.66
7	0.275	0.4375	0.5	0.99	0.4	0.94
			0.6	0.90	0.5	0.86
			0.7	0.82	0.6	0.82
		0.60	0.5	1.38	0.4	1.32
			0.6	1.28	0.5	1.22
			0.7	1.16	0.6	1.16

waveforms, and its ability to correctly predict the change in pulse amplitude and waveform as it traverses the combustion chamber (over several wave cycles).

Motor Response to Ejecta Pulsing

Triggered nonlinear instabilities were observed in all of the tests shown in Table 4. In tests 1, 2, 3, 8, and 9, the first ejecta triggered the instability, while in tests 4-7 the motor was stable in response to the first pulse but unstable in response to the second pulse. It has been observed that the amplitude of the oscillations increased as the grain was lengthened. Small increases in mean chamber pressure (dc shift) were observed whenever the unstable oscillations were induced. The dc shift also increased in magnitude as the length of the test grain was increased. In addition, significant changes in the oscillation's waveform were observed. As the grain was lengthened, the waveform became narrower and steeper (both front and back). Thus, it was concluded that longer grains are capable of sustaining waves with considerably more high-frequency content that shorter grains.

In Ref. 7, the nonlinear model was utilized to predict the response of solid rocket motors to piston, low brisance, and pyrotechnic pulsers. Excellent agreement between the measured and predicted motor response was demonstrated. As explained therein, present deficiencies in combustion response modeling require that some of the parameters in the transient combustion models be empirically adjusted to best fit the experimental data. In the piston and pyro pulsing investigation, the constants were determined from one test and were used successfully in predicting the results of five other pulses. The motors and propellant used in this previous study were the same as used herein, except that the grain lengths were not significantly varied (8-9 in.), and the motors were pulsed at considerably higher chamber pressures (1500-1900 psi). Results obtained using the nonlinear model to predict motor response to ejecta pulsing are discussed below.

Figures 8-11 show comparisons between the predicted and measured head-end pressure oscillations for tests 1, 6, 7, and 9. Since the ejecta tests used the same propellant as the earlier piston and pyro pulser tests, the initial ejecta calculations were made using the same combustion response parameters. The final solutions shown in these figures employed the same

Table 4 Comparison of measured and predicted pulse amplitudes (in percentage of mean pressure) at the head-end closure

Test No.	Head end	
	Measured	Predicted
1 first pulse	3.4	3.5
2 first pulse	3.6	3.7
3 first pulse	1.7	1.8
4 first pulse	1.6	1.6
5 first pulse	3.9	3.8
5 second pulse	9.6	10.8
6 first pulse	4.4	4.7
6 second pulse	9.7	10.2
7 first pulse	5.9	6.1
7 second pulse	9.2	10.3
8 first pulse	6.6	7.8
9 first pulse	19.9	22.7

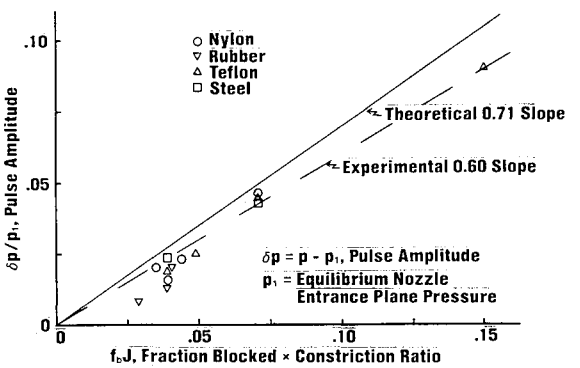

Fig. 7 Ejecta pulse amplitude vs fraction of throat area blocked times constriction ratio.

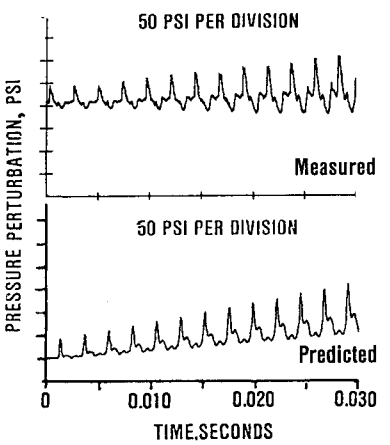

Fig. 8 Comparison of measured and predicted pressure perturbations at the head end, test 1.

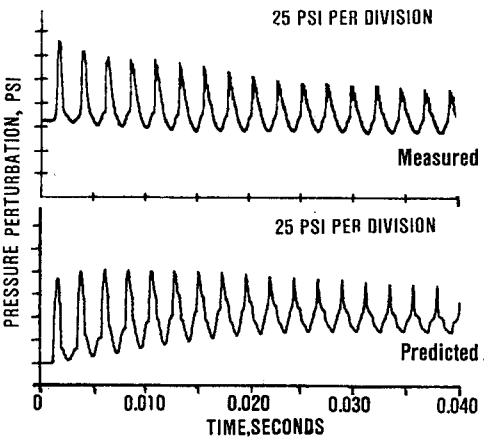

Fig. 9 Comparison of measured and predicted pressure perturbations at the head end, test 6, second pulse.

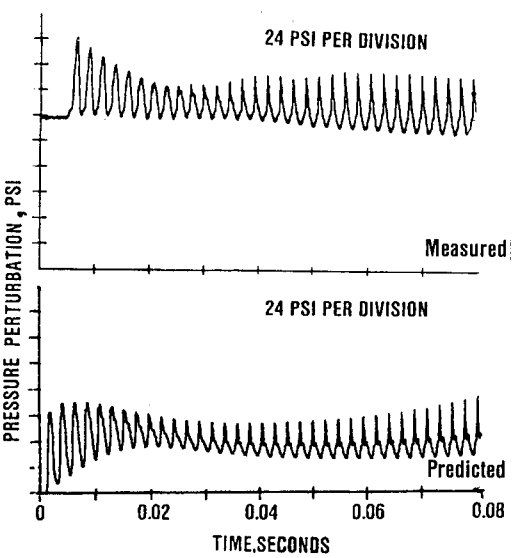

Fig. 10 Comparison of measured and predicted pressure perturbations at the head end, test 7, second pulse.

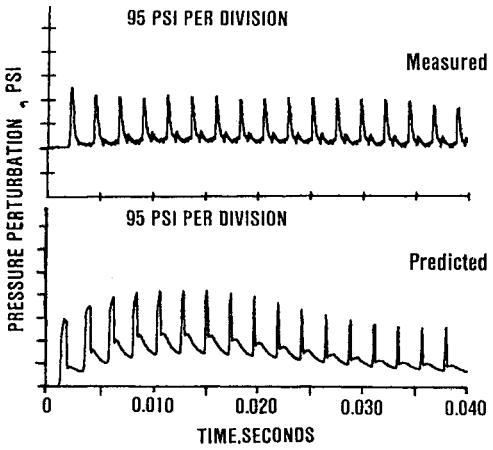

Fig. 11 Comparison of measured and predicted pressure perturbations at the head end, test 9, second pulse.

values for the parameters that determine the pressure-coupled response. Nevertheless, as expected, the velocity-coupled response function had to be varied as the grain length varied in order to achieve best agreement with the data. The ad hoc velocity coupling formulation used in the present analysis[10] does not model the governing fundamental physical mechanisms (which remain to be identified). Thus, the fact that it cannot predict the proper variation of velocity coupling with grain length should not be surprising.

The velocity-coupled response functions used in the predictions ranged from 2.9 to 4.6. In general, the longer the grain, the lower the value of R_{vc} used. In Ref. 7, a value of R_{vc} equal to 3.5 was used with 8-in. long grains; however, the chamber pressure in the earlier tests was about double that of the present tests.

In test 1, the motor was driven unstable by the first pulse. At this time in the firing, the partial grain is not flush with the chamber wall. As discussed in previous work,[7] the area discontinuity causes multiple reflections of the primary shock wave as it traverses the chamber. Figure 8 shows that the analysis predicts the observed occurrence of multiple waves (one reflection before and one reflection following the primary shock wave), and also shows the ability to predict the observed growth rate of the oscillations. It should be mentioned that the changes in mean chamber pressures (dc shifts) observed in some of the theoretical predictions, were also observed in the experimental data but were filtered out. The theoretical and experimental dc shifts were of comparable magnitudes.

Figures 9 and 10 for tests 6 and 7, respectively, demonstrate the effect of ejecta density on motor response. Both motors were stable in response to the first pulse and unstable in response to the second pulse. As previously discussed, the teflon (test 6) and steel (test 7) ejecta both produced approximately the same initial pulse amplitude (at the nozzle entrance), however, the lighter teflon ejecta produced a much narrower pulse than the steel ball. The teflon induced pulse is already shocked by the time the pulse reaches the head end of the motor. As time progresses, the pulse slowly widens and decays in amplitude until a limit cycle amplitude and waveform are achieved. The response to the steel ejecta is considerably more complex. The steel induced initial waveform is almost a pure fundamental mode disturbance with very little higher harmonic content. The transformation to a steep-fronted wave takes about nine wave cycles (during which time the amplitude decays continously). Only when the wave becomes a traveling shock does it begin to grow. As the wave grows it changes shape and eventually reaches approximately the same limiting amplitude and waveform as the teflon pulsed motor.

The predicted behavior for tests 6 and 7 (shown in Figs. 9 and 10) closely parallels the observed motor response. The initial pulse amplitude and waveform, the time evolution of the pressure wave and limiting amplitude are all reproduced correctly. The ability of the analysis to correctly reproduce the complex behavior of test 7 was particularly gratifying.

Figure 11 shows the pressure data measured at the head end for test 9 (full-length grain). The first ejecta produced a narrow pulse, with measured amplitude at the head-end closure of 250 psi. The pulse initiated a sustained instability in the motor. The waveform development in this case was distinctly different from that in motors with short partial-length grains. The narrow initial pulse became even a narrower, spike-like wave followed by a small second compression wave. The full-length grain also produced a substantially larger mean pressure increase (dc shift) than the partial length grains. The dc shift of about 10% is not apparent in the experimental data because the dc pressure component of the transducer signal has been filtered out. The dc shift is apparent in the calculated results which, in addition to predicting the observed mean pressure shift, also correctly predict the initial and fully developed waveforms and amplitudes.

Although not shown herein, good agreement was also obtained between the predicted and measured results for tests 2-5 and 8. In all cases where the first pulse was stable and the second unstable (tests 4-7), the analyses correctly predicted that behavior without any need to adjust the combustion response parameters. It should also be mentioned that tests 6 and 7 are two of the best examples, to date, of experimental evidence supporting previous analytical predictions that the limit cycle is independent of the characteristics of the initiating disturbance.

Summary and Conclusions

A series of ejecta pulsed motor firings was conducted in simple laboratory-scale motors with full- and partial-length cylindrical grains. Ejecta size and density were varied to provide information on the effect of these parameters on pulse amplitude, pulse waveform, and the ability to trigger nonlinear instability. Each of the motors was pulsed twice, and all were triggered into sustained nonlinear instability.

A simple trajectory analysis was developed to calculate the velocity of the ejecta as it transits the nozzle. The model considers only the drag force on the ejecta and neglects effects due to gas flow pressure gradients and ejecta-flowfield interactions. Relatively good agreement between predicted and measured pulse durations was obtained. Parametric calculations demonstrated that the pulse duration is only weakly dependent on initial ejecta velocity and the value used for the drag coefficient; thus, an effort to develop a more complete model of the ejecta dynamics does not appear to be warranted.

Two models for predicting ejecta pulse amplitudes were developed. A simple model based on linear wave propagation theory and the assumption of quasisteady nozzle behavior, and a numerical model which utilizes the quasisteady nozzle assumption to provide a nozzle entrance boundary condition for a comprehensive nonlinear instability analysis. The simple model is limited to the prediction of the ejecta induced pulse amplitude at the nozzle entrance plane. The numerical model is more complete and can predict the initial pulse amplitude and waveform at all locations in the motor (not just the nozzle entrance plane) as well as the temporal and spatial evolution of the pulse, i.e., the motor response to ejecta pulsing. The simple method predicts the pulse amplitude to be proportional to the product of the fraction of the nozzle area blocked and the initial constriction ratio of the nozzle $\delta p/p = 0.71 f_b J$. A semiempirical expression of the form $\delta p/p = 0.6 f_b J$ yields a good correlation of the data, supporting the validity of the analysis and demonstrating that the quasisteady assumption leads to overprediction of pulse amplitude. As ejecta size

decreases, velocity increases and pulse duration decreases. When pulse duration is decreased to the range of about 0.2-0.4 ms, the data are better correlated by $\delta p/p = 0.4 f_b J$. Comparisons with data verified the ability of the analysis to predict the observed waveforms, and its ability to correctly predict the change in pulse amplitude as it traverses the combustion chamber.

The test results demonstrated that both pulse amplitude and pulse duration influence the ability of a pulse to trigger instability (higher amplitudes and shorter pulse durations enhance triggering potential). The observed greater susceptibility of motors to triggering at later burn times agrees with many other previous observations. Oscillation amplitudes, dc shifts, and amount of high-frequency content were all observed to increase with increase of grain length (in a motor of fixed length). The existence of area discontinuities, when the partial length grains are not flush with the case, results in multiple wave reflections, which, in general, make it more difficult to trigger such configurations into instability.

The wide range of waveforms and nonlinear behavior observed in the experiments results from interactions between a number of complex nonlinear physical phenomena. Comparisons between predictions obtained with the present nonlinear instability analysis and the experimental data indicate that the model is capable of predicting most of the observed characteristics, i.e., pulse amplitude and waveform, waveform evolution, growth rate, dc shifts, waves that decay and then grow (and vice versa), etc.

Although the present analysis appears to contain all of the esssential factors necessary to produce the observed nonlinear behavior of solid rocket motor instabilities, the results of the present comparison study, in which grain lengths were systematically varied, point out deficiencies in the existing modeling of the effect of acoustic velocity oscillations on the combustion response of the propellant (velocity coupling). The present predictions require empirical adjustment of the velocity-coupled response to obtain the best possible agreement. Further progress in the understanding and modeling of the physical mechanisms which govern the combustion response of solid propellants must be accomplished before quantitative, a priori stability predictions can be obtained.

Acknowledgments

The authors wish to express their gratitude to James S. B. Chew for his assistance in the preparation of the figures. This work was partially supported under U.S. Air Force Contract F04611-81-C-0007.

References

[1] Combs, L. P. et al., "Improvement of Bombs and Pulse Guns as Combustion Stability Ratings Devices," AFRPL-TR-68-018, March 1968.

[2] Dickinson, L. A., "Command Initiation of Finite Wave Axial Combustion Instability in Solid Propellant Rocket Motors," *ARS Journal,* Vol. 32, 1962, p. 643.

[3] Morris, E. P., "A Pulse Technique for the Evaluation of Combustion Instability in Solid Propellant Rocket Motors," *CAS Journal,* 1965, pp. 329-333.

[4] Murray, J. A. et al., "Pulsing Criteria for Solid Rocket Motor," Volume I, Final Report, and Volume II, "Motor Pulsing Design Manual," AFRPL-TR-79-45, March 1981.

[5] Lovine, R. L., "Nonlinear Stability for Tactical Motors-Pulsing Considerations," presented at the 18th JANNAF Combustion Meeting, Pasadena, Calif., Oct. 1981, CPIA Rept. 347, 1981.

[6] Baum, J. D., Levine, J. N., and Lovine, R. L., "Pulsing Techniques for Solid Propellant Rocket Motors; Modeling and Cold Flow Testing," *Journal of Spacecraft and Rockets,* Vol. 20, March-April 1983, pp. 150-157.

[7] Baum, J. D., Levine, J. N., and Lovine, R. L., "Pulse Triggered Instability in Solid Rocket Motors," AIAA Paper 82-1219, Cleveland, Ohio, June 1982.

[8] Levine, J. N. and Baum., J. D., "Modeling of Nonlinear Combustion Instability in Solid Propellant Rocket Motors," *Proceedings of the Nineteenth Symposium (International) on Combustion,* Haifa, Israel, Aug. 1982, pp. 769-776.

[9] Schlichting, H., *Boundary Layer Theory*, 7th Ed., McGraw-Hill Book Co., New York, 1979.

[10] Levine, J. N. and Baum, J. D., "A Numerical Study of Nonlinear Instability Phenomena in Solid Rocket Motors," *AIAA Journal,* Vol. 21, April 1983, pp. 557-564.